Monthly Notices of the ROYAL ASTRONOMICAL SOCIETY

MNRAS **498,** 3658–3663 (2020) doi:10.1093/mnras/staa2574
Advance Access publication 2020 August 24

Proxima Centauri – the nearest planet host observed simultaneously with *AstroSat*, *Chandra*, and *HST*

S. Lalitha [1]★ J. H. M. M. Schmitt,[2] K. P. Singh,[3] P. C. Schneider,[2] R. O. Parke Loyd,[4] K. France,[5] P. Predehl,[6] V. Burwitz[6] and J. Robrade[2]

[1]*School of Physics & Astronomy, University of Birmingham, Edgbaston, Birmingham B15 2TT, UK*
[2]*Hamburger Sternwarte, University of Hamburg, Gojenbergsweg 112, D-21029 Hamburg, Germany*
[3]*Indian Institute of Science Education and Research Mohali, Sector 81, SAS Nagar, Manauli, PO 140306, India*
[4]*School of Earth and Space Exploration, Arizona State University, Tempe, AZ 85287, USA*
[5]*Laboratory for Atmospheric and Space Physics, University of Colorado, 600 UCB, Boulder, CO 80309, USA*
[6]*Max-Planck-Institut für Extraterrestrische Physik, D-85748 Garching, Germany*

Accepted 2020 August 14. Received 2020 August 11; in original form 2020 June 7

ABSTRACT

Our nearest stellar neighbour, Proxima Centauri, is a low-mass star with spectral type dM5.5 and hosting an Earth-like planet orbiting within its habitable zone. However, the habitability of the planet depends on the high-energy radiation of the chromospheric and coronal activity of the host star. We report the *AstroSat*, *Chandra*, and *HST* observation of Proxima Centauri carried out as part of the multiwavelength simultaneous observational campaign. Using the soft X-ray data, we probe the different activity states of the star. We investigate the coronal temperatures, emission measures and abundance. Finally, we compare our results with earlier observations of Proxima Centauri.

Key words: stars: activity – stars: coronae – stars: individual: Proxima Centauri – stars: late-type – stars: low-mass .

1 INTRODUCTION

The habitability of an extrasolar planet depends not only on its distance from its host but also on the host's magnetic activity. The host's high-energy emission in the X-ray and UV-range determines the amount of mass-loss from the planetary atmosphere (Lammer et al. 2003); given some incident high-energy flux, evaporation takes place in the form of 'hydrodynamic escape'. The nearest extrasolar planet orbits around the star Proxima Centauri, which itself is located in a hierarchical triple system consisting of Proxima Centauri and a closer binary α Centauri AB (with components of spectral type G2V and K1V). Proxima Centauri is an M-dwarf of spectral type dM5.5e (Shapley 1951).

Some solar flares are known to be associated with coronal mass ejection when suddenly energetic particles are released into interplanetary space. If and when such particles enter the Earth's magnetosphere, geomagnetic disturbances of various strengths are observed. By analogy, we may expect analogous events in the Proxima Centauri planetary system, and recently a superflare event on Proxima Centauri has been reported, which would have been barely visible with the naked eye (Howard et al. 2018); we summarize some of the relevant stellar parameters of Proxima Centauri in Table 1.

Proxima Centauri, like all flare stars, is a copious producer of X-ray and UV emission. It has therefore been observed frequently by several X-ray (and UV satellites) such as *Einstein*, EXOSAT, *ROSAT*, *ASCA*, *Chandra*, and *XMM–Newton* (Haisch & Linsky 1980; Haisch et al. 1983; Haisch, Antunes & Schmitt 1995; Güdel et al. 2004). Proxima Centauri's quiescent X-ray emission varies from 4 to 16 $\times$ 10^{26} erg s^{-1} (Haisch et al. 1990). Although its surface area is much smaller than that of our Sun, its X-ray emission is usually quite a bit larger. Frequent flaring is observed from Proxima Centauri in optical, UV, X-ray, and radio wavelengths, with several flares studied in detail over the over last four decades (Haisch et al. 1983; Lim, White & Slee 1996; Güdel et al. 2002; Fuhrmeister et al. 2011; MacGregor et al. 2018). Furthermore, based on 15 yr All Sky Automated Survey (ASAS) *V*-band data Wargelin et al. (2017) found that Proxima Centauri shows a ∼7 yr modulation with similar indications of activity cycle in X-ray wavelength.

Currently, we do not have a reliable method to estimate the energetic particle output of magnetically active late-type stars. It is, however, possible to measure the radiative output and assess the planetary evaporation due to incident high-energy radiation. To assess the full high-energy radiation field between 5 and 3200 Å one has to combine the UV and X-ray observations. Since most of the radiation in the EUV range (150 Å $< \lambda <$ 911 Å) is obscured by the interstellar medium even for the very nearest stars like Proxima Centauri, we require simultaneous X-ray and UV/optical observations as well as emission measure modelling to reconstruct the coronal contribution to the EUV flux. We present a detailed analysis of coronal emission of Proxima Centauri during both quiescent and flaring states observed simultaneously with *AstroSat* Soft X-ray Telescope (SXT; Singh et al. 2014, 2016), *Chandra* Low Energy Transmission Grating (LETG/HRC-S; Brinkman et al. 1987, 1997) and *Hubble Space Telescope* (*HST*) .

Our paper is structured as follows: In Section 2, we describe our observations obtained with *AstroSat* and the data analysis. In Section 3, we compare the timing behaviour of Proxima Centauri observed

★ E-mail: sairaml@bham.ac.uk

Table 1. Properties of star systems and the *AstroSat* observations.

Proxima Centauri		
Distance (pc)	1.3	a
Spectral type	dM5.5e	b
Rotation period (d)	83	c
L_X (erg s^{-1})	4–16 × 10^{26}	d
L_{bol} (erg s^{-1})	6 × 10^{30}	e
$\frac{L_X}{L_{bol}}$	−4	
Proxima Centauri b		
Mass ($M_\oplus$)	∼1.3	e
Orbital period (d)	∼11.2	e
Semimajor axis a (au)	∼0.05	e
AstroSat		
Observation start	31/05/2017 06:08:50	
Observation end	01/06/2017 13:51:33	
Duration (ks)	∼42	
Primary instrument	SXT	
ObsID	A03 − 046T01 − 9000001260	
Chandra		
Observation start	31/05/2017 16:25:42	
Observation end	01/06/2017 05:28:58	
Duration (ks)	45	
Primary instrument	LETG/HRC-S	
ObsID	19708	

Note. References: (a) van Leeuwen (2007), (b) Boyajian et al. (2012), (c) Kiraga & Stepien (2007), (d) Haisch et al. (1990), Reid et al. (2001), (e) Anglada-Escudé et al. (2016).

with *AstroSat* and zeroth-order LETG/HRC-S observations. We also briefly present the *HST* observation of the flare event that was seen simultaneously with *AstroSat* and *Chandra*. We further discuss the coronal properties of Proxima Centauri and verify the consistency of the results with the LETG/HRC-S observations. In Sections 4, we summarize our findings.

2 OBSERVATIONS AND DATA ANALYSIS

The data presented in this paper are simultaneous observations of Proxima Centauri carried out with India's first space observatory *AstroSat*, the LETG/HRC-S onboard *Chandra* and *HST* (ObsID: 14860) between 2017 May 31 and June 1. The observations cover 19 consecutive *AstroSat* orbits. The detailed observation log are provided in Table 1.

AstroSat is a multiwavelength astronomy mission, carrying five multiband payloads (Agrawal 2006; Singh et al. 2014; Agrawal 2017). The SXT aboard *AstroSat* covers the 0.3–7.0 keV energy band with an effective area of ∼90 cm^2 at 1.5 keV (Singh et al. 2017b). The SXT is a grazing incidence soft X-ray telescope with a focal length of 200 cm, equipped with a thermo-electrically cooled CCD detector in its focal plane (Singh et al. 2014, 2016, 2017a, b). The SXT level 1 data from individual orbits are received at the SXT Payload Operation Centre (POC) and are processed using the SXTPIPELINE version 1.4b at the POC. Using the SXTPIPELINE the events are extracted and time tagged, and the raw coordinates are transformed to sky coordinates. The pipeline also carries out bias subtraction, bad pixel flagging, event grading, and pulse height amplitude reconstruction for each event. So-called Good Time Interval files for each orbit are selected and merged event files are created.[1]

[1]http://www.tifr.res.in/∼astrosat_sxt/dataanalysis.html

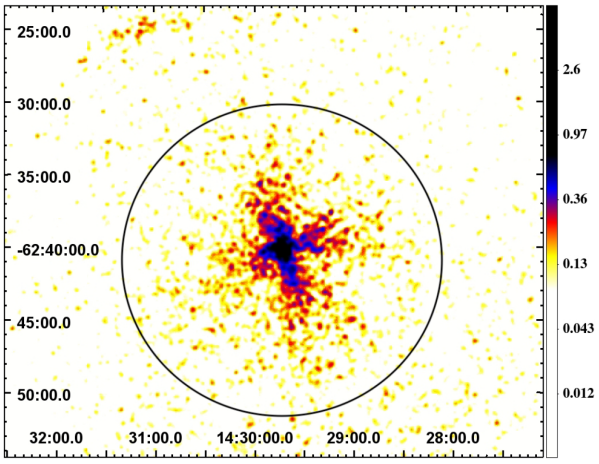

Figure 1. Soft X-ray image of Proxima Centauri merged soft X-ray data in the 0.5–4 keV energy band. The black circle represents the source signal extracted from a circular region with 12 arcmin radius.

We used XSELECT version 2.4c in HEASOFT 6.24 to extract the light curve for the regions centred on the sources. The SXT light curves and spectra were obtained using standard filtering criteria.[2] We used a blank-sky SXT spectrum provided by the SXT team for modelling the background spectrum. We used the XSPEC-compatible RMF and ARF files for SXT provided by the *AstroSat* Science Support cell[3]. These were sxt_pc_excl00_v04_a.arf and sxt_pc_mat_g0to12.rmf. The spectra were binned to a minimum of 25 counts per energy bin. The spectral analysis was carried out with XSPEC version 12.9.0 (Arnaud 1996) after dividing the data into periods of quiescence and flaring (see Sections 3.1 and 3.2).

For the *Chandra* data, we followed the standard CIAO analysis guide[3] for reducing *Chandra* LETG/HRC-S data. We used CIAO version 4.10 of the data processing software. According to the standard data processing procedure the Good Time Interval files were created.

Proxima Centauri was simultaneously observed using the STIS spectrograph aboard *HST* with the E140M echelle grating. To produce flux and wavelength calibrated spectra, we used the standard `calSTIS` pipeline version FIXME. We split the *HST* observations into sub-exposures with the `calSTIS inttag` function at a cadence of FIXME, resulting in individual spectra for each of these sub-exposures. From these spectra, we integrated flux from 1200 to 1700 Å region to generate a broad-band FUV light curve.

3 RESULTS

To provide an impression of what *AstroSat* data look like, we show our *AstroSat*-SXT image of Proxima Centauri in Fig. 1. The source signal was extracted from a circular region with 12 arcmin radius centred on the proper-motion corrected and nominal position of Proxima Centauri.

3.1 X-ray light curves

In Fig. 2 (black data points), we plot the background-subtracted SXT light curves for Proxima Centauri binned by 100 s over the

[2]http://astrosat-ssc.iucaa.in/?q=data_and_analysis
[3]http://cxc.harvard.edu/ciao/guides/

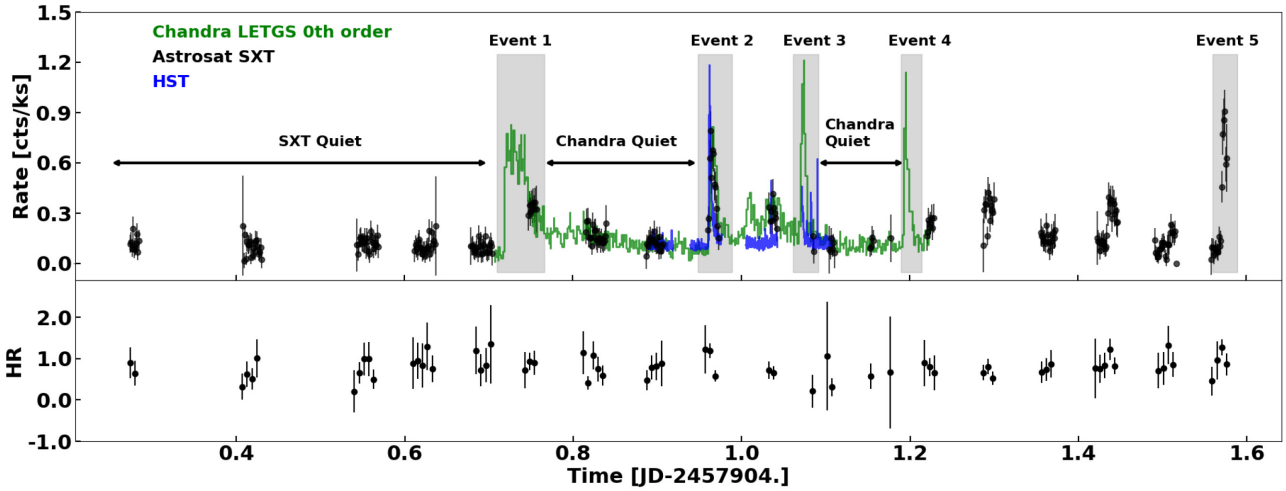

Figure 2. Top panel: *Astrosat* SXT (black) and *Chandra* LETG/HRC-S zeroth-order (in green) light curves of Proxima Centauri plotted in 0.3–3.0 keV energy band binned to 100 s. The scaled *HST* light curve is represented in blue. Plotted in the bottom panel is the *Astrosat* SXT hardness ratio binned to 500 s. The time segments corresponding to the flare-like events are represented by the vertical blocks.

entire 110 ks observing period by *AstroSat*; the obtained zeroth-order LETG/HRC-S light curve is also shown as green data points. Fig. 2 clearly shows the different observation patterns followed by *AstroSat* and *Chandra*; the *AstroSat* data stream is frequently interrupted by Earth blocks, while the *Chandra* data stream is continuous. Fortuitously, the count rates measured by both instruments are very similar. Although the HRC-S has no useful energy resolution in zeroth order, we can study spectral variability by using the SXT data to create hardness ratios (HR). It is defined as the ratio between the counts in the hard band (1.0–3.0 keV) and the soft band (0.3–1.0 keV). In Fig. 2 bottom panel, the HR binned to 500 s is plotted. Due to the sparse sampling of the HR plots, we do not see any heating related trends.

Several energetic events can be seen in both *AstroSat* and *Chandra* light curves, we call them Events 1–5. There are four flare-like events seen in the *Chandra* light curve, we call them Events 1–4. The peak count rate of Event 1, 3, and 4 observed in *Chandra* light curves are ∼0.75, ∼1.23, and ∼1.18 cts s^{-1}, respectively. Event 2 which occurred around JD∼2457904.94 was covered by both X-ray instruments as well as *HST*. During Event 2 the count rate increased from the quiescent value of ∼0.13 to ∼0.80 cts s^{-1} in both *Chandra* and SXT light curves in 0.5–4.0 keV range. Correspondingly, during the flare the *HST* light curve shows that the normalized flux increases by two orders of magnitude. The Event 2 occurs over ∼2700 s producing integrated energy of $\sim 4.7 \times 10^{30}$ erg in 0.5–4.0 keV (see Section 3.2 for discussion of spectral fitting). The energetics of the Event 2 indicates a moderate flare in comparison to the very strong flare studied by Güdel et al. (2004) with a total energy of $\approx 2 \times 10^{32}$ erg and several other flares with energies of the order of 10^{31} erg studied by Fuhrmeister et al. (2011). Furthermore, we note an increased activity state of Proxima Centauri towards the end of *AstroSat* observations which we call Event 5. The count rate reaches a maximum of ≈0.90 cts s^{-1}. However, since the observations ended during the event we did not carry out further analysis.

3.2 Spectra

We extracted the quiescent and flaring interval spectra of Proxima Centauri to study the emission measure and coronal elemental abundance changes as a result of the flares. In Fig. 3 (left-hand panel), we plot the SXT spectra during quiescence (black data points) and Event 2 (red data points).

The *Chandra* LETG/HRC-S zeroth-order light curve shows a large number of flaring events. The Event 2 observed by *AstroSat* SXT has been observed by *Chandra* LETG/HRC-S as well, however, the signal-to-noise ratio for LETG/HRC-S spectra was not adequate for the spectral fit. Hence, we combined all the LETG flare data (Events 1–4) for fitting and selected two time periods in the remaining data (marked as 'Chandra Quiet' in Fig. 2) to create a quasi-quiescent spectrum. In Fig. 3 right-hand panel, we show the *Chandra* integrated spectra of the quiescent and combined Events 1–4. We fit the LETG/HRC-S spectra in 0.206–7.0 keV range for the positive order and 0.252–7.0 keV range for the negative order independently for the flare and quiescent time intervals.

Using XSPEC, we performed a global fit to the SXT spectra using APEC plasma models[4] to the SXT spectra. To compare the quiescent and the flaring state we defined a fixed temperature grid with values 0.5, 1.0, and 2.0 keV (5.7, 11.5, and 23 MK, respectively). In these fits, the determined abundances are relative to solar values Grevesse & Sauval (1998), and all three-temperature components share the same abundance. We allowed the abundance to vary independently to fit the quiescent and flare spectra. Assuming a distance of ∼1.3 pc, we also calculate the emission measure from the component's normalization. Similar to SXT spectra, we fit the quiescent and the Events 1–4 observed with *Chandra* with three-temperature APEC models allowing the abundance to vary freely. The resulting fit parameters are given in Table 2.

Although the three-temperature component APEC may be adequate to interpret the spectra observed with SXT, the assumption of three discrete temperatures is not realistic to physically describe the stellar coronae. Hence, we also experimented with a more complex model such as a c6pmekl[5] which uses sixth-order Chebyshev polynomial describing differential emission measure (Lemen et al. 1989; Singh, White & Drake 1996). However, we found that the three-temperature model described above provides a reasonable description of our data.

[4] https://heasarc.gsfc.nasa.gov/xanadu/xspec/manual/node135.html
[5] https://heasarc.gsfc.nasa.gov/xanadu/xspec/manual/node149.html

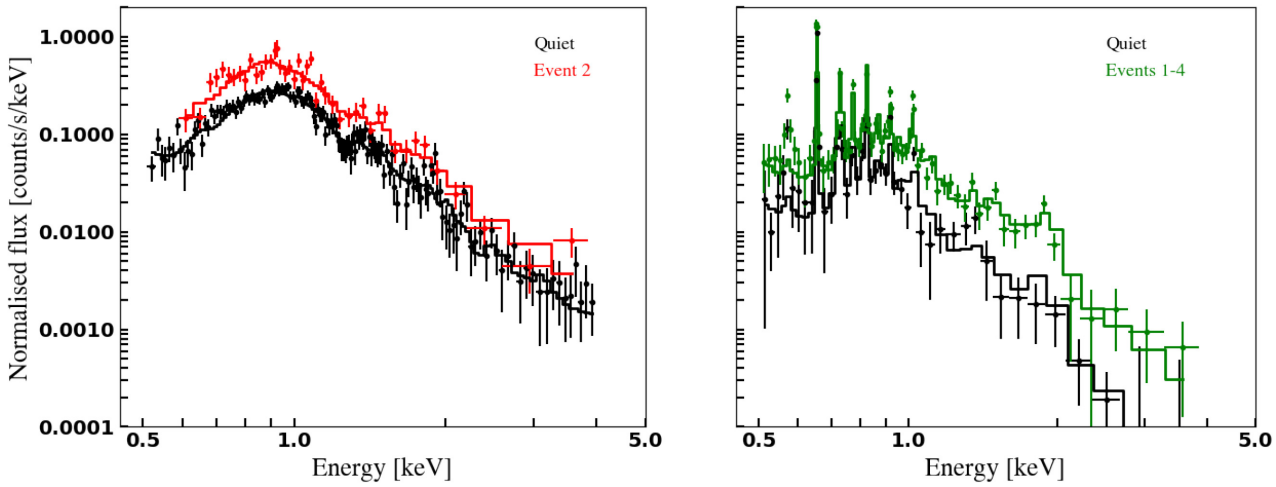

Figure 3. Left-hand panel: *AstroSat* SXT spectra of Proxima Centauri during quiescent (black) and flare (red) in 0.5–4.0 keV. Right-hand panel: *Chandra* LETG/HRC-S spectra integrated spectra of quiescent duration (black) and combined flaring Events 1–4 (green).

Table 2. Three-temperature fit to the *AstroSat* SXT and *Chandra* LETG/HRC-S spectra in the energy range 0.5–4.0 keV during different activity states allowing individual elemental abundance and emission measure to vary. Errors given are 1σ errors.

Parameter	LETG/HRC-S		*AstroSat*	
	Quiet	Events 1–4	Quiet	Event 2
T_1 (keV)	0.5	0.5	0.5	0.5
T_2 (keV)	1.0	1.0	1.0	1.0
T_3 (keV)	2.0	2.0	2.0	2.0
EM_1 (10^{49} cm^{-2})	$2.16^{+1.71}_{-1.61}$	$2.04^{+1.38}_{-0.97}$	$3.99^{+2.28}_{-1.62}$	$9.88^{+7.47}_{-4.43}$
EM_2 (10^{49} cm^{-2})	$2.64^{+1.15}_{-1.42}$	$3.76^{+4.92}_{-3.58}$	$13.21^{+4.93}_{-5.41}$	$15.47^{+6.63}_{-8.43}$
EM_3 (10^{49} cm^{-2})	$5.93^{+1.40}_{-1.28}$	$5.14^{+2.79}_{-3.93}$	$10.81^{+2.42}_{-3.64}$	$12.32^{+4.32}_{-6.99}$
Abundance[a]	$0.23^{+0.86}_{-0.12}$	$0.35^{+0.08}_{-0.09}$	$0.38^{+0.14}_{-0.10}$	$0.32^{+0.31}_{-0.16}$
Flux $\times 10^{-12}$ (erg s^{-1} cm^{-2})	3.52 ± 0.58	7.85 ± 0.75	5.13 ± 0.72	15.59 ± 1.56
L_X (10^{27}erg s^{-1})	0.71 ± 0.11	1.58 ± 0.15	1.03 ± 0.15	3.15 ± 0.32
χ^2	1.77	1.93	1.12	1.23

[a]Relative to solar photosphere.

During a flare, fresh chromospheric material unaffected by elemental differentiation (first ionization potential effect also known as 'FIP effect') is expected to be evaporated and transported into the corona, thus changing the coronal emission measure and potentially some element abundances (Ottmann & Schmitt 1996; Benz & Güdel 2010). In a moderately active M star such as Proxima Centauri, during quiescent emission, a pronounced anti-FIP effect is expected (Wood & Linsky 2010; Fuhrmeister et al. 2011), but uncertainties for the abundances during quiescence and flaring were too large in our fits to detect any differences.

Since the quantum efficiency and the effective area of X-ray instruments are not uniform over energy bands, we compare the *Chandra* LETG/HRC-S and *AstroSat* SXT in smaller segments of energy bandpasses. We used the quiescent spectra of both the instruments in five energy bandpasses 0.5–1.0, 1.0–1.5, 1.5–2.0, 2.0–4.0, and 4.0–7.0 keV. We fit three-temperature APEC models and ignored all the data points out of the energy band of interest. We note that the LETG/HRC-S above 2 keV is not useful due to statistical limitations. The flux ratio between the *AstroSat* SXT and *Chandra* LETG/HRC-S produces a difference $>1.5\sigma$. The difference in the fluxes could be inherent due to the difference in the time periods chosen for the spectra. Furthermore, since the calibration to convert the counts into absolute fluxes are not very accurate, this can also result in the discrepancies when we compare the fluxes from different instruments.

3.3 Simultaneous observation

In Fig. 4, we show a close-up view of Event 1 observed simultaneously with *AstroSat* SXT, *Chandra* LETG/HRC-S, and *HST* binned to 100s each. The vertical lines in brown and yellow represents the UV and X-ray flare peaks, respectively. The amplitudes of the *HST* light curves are scaled to be consistent with X-ray light curves. A detailed analysis of the *HST* data will be presented in Schneider et al. (in preparation). However, a visual inspection of Fig. 4 indicates that the *HST* FUV light curve precedes the X-ray light curves by about a few minutes. This may indicate that the presence of Neupert effect (Neupert 1968) during the rising phase of Event 2. Using the Z-transformed discrete correlation function (ZDCF) (Alexander 1997), the cross-correlation of the *HST* and the X-ray light curves produces a time-lag between the peaks to be 300–400 s, indicating that due to electron impingement the UV light curve precedes the thermal radiation.

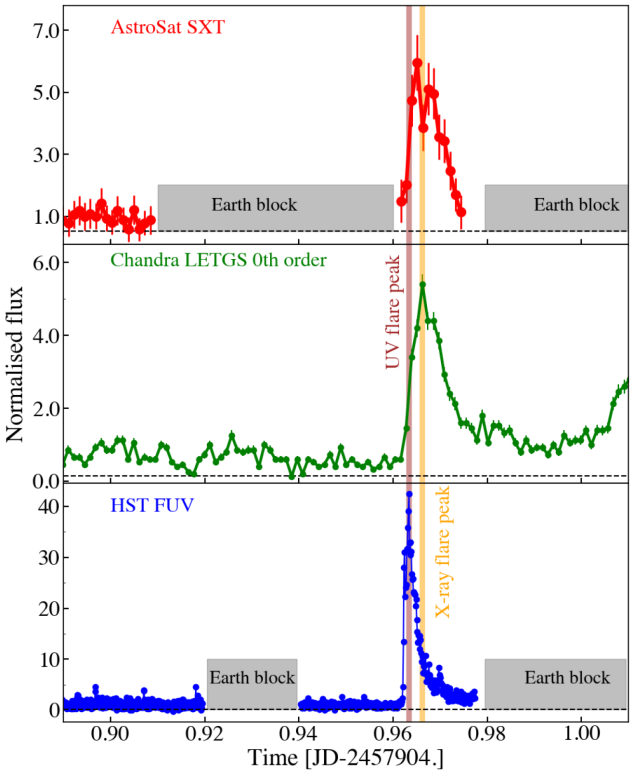

Figure 4. Event 2 simultaneously observed with the *AstroSat* SXT in 0.5–4.0 keV (top panel), *Chandra* LETG/HRC-S zeroth order in 0.1–12.0 keV (middle panel), and *HST* FUV in 120–170 nm (bottom panel).

3.4 Comparison

The quiescent emission measured with *Einstein*, EXOSAT, and *ROSAT* in 0.3–4.0 keV energy ranges are 7.2×10^{-12}, 4–16 $\times 10^{-12}$, and 2.6–7.2 $\times$ 10^{-12} erg s^{-1} cm^{-2}, respectively. The quiescent X-ray flux observed by *Einstein* and EXOSAT was reported by Haisch & Linsky (1980) and Haisch et al. (1990), respectively. We used the *ROSAT* observations listed in the *ROSAT* Positive Sensitive Proportional Counter source catalogue (Voges et al. 1996, 2000). Assuming a coronal temperature of 1 keV, sub-solar abundance of 0.5 and using WebPIMMS, we computed energy conversion factor $\mathrm{ECF_{PSPC}} = 6.4 \times 10^{-12}$ erg cm^{-2} counts^{-1} to convert the observed *ROSAT* counts to flux in canonical 0.1–2.4 keV *ROSAT* energy band. Furthermore, we use the X-ray flux reported by Fuhrmeister et al. (2011) based on *XMM–Newton* observations. In Fig. 5, we plot quiescent flux measured between 1979 and 2017 as a function of time. Furthermore, we assume similar temperature and abundance as before and used WebPIMMS to estimate the flux in the 0.3–4.0 keV energy range. The flux obtained from *AstroSat* is consistent with the previous estimates of quiescent flux for Proxima Centauri.

While a clear cyclic behaviour with a period of ∼7.0 yr is observed for Proxima Centauri in ASAS observations, a similar variation in the X-ray data is not apparent immediately. However, Wargelin et al. (2017) reported the evidence for a 7 yr stellar cycle using observations from several X-ray missions, principally *Swift*. The temporal coverage of X-ray observation, the energy resolution and uncertainties due cross-calibration restrict a detailed analysis of the cyclic behaviour of Proxima Centauri. However, we performed a periodogram analysis of all the compiled X-ray data, but we were unable to obtain a significant peak indicating a period. We used the 7 yr period obtained from the optical light curve obtained based

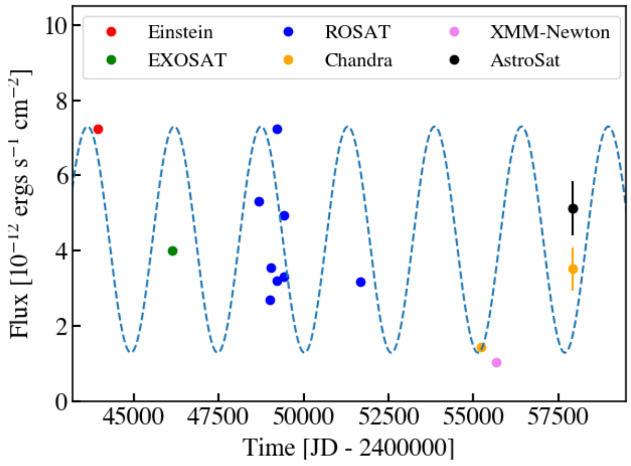

Figure 5. Quiescent emission flux as a function of time in 0.3–4.0 keV energy range observed by several X-ray missions between 1979 and 2017. An arbitrary sine curve with a period of 7 yr is represented as the blue dashed curve.

on ASAS observations reported by (Suárez Mascareño, Rebolo & González Hernández 2016). We assumed that the optical period also applies to the X-ray data and plot a sinusoidal curve with a period of 7 yr in Fig. 5. Furthermore, assuming that the optical cycle also applies to the X-ray cycle, we carried out a correlation analysis between the two data sets. We used the fitted optical light curve at each X-ray observation, to relate the X-ray observations to the measured optical magnitude. We computed the linear Pearson correlation coefficient (ρ) of −0.42 between the X-ray flux and the optical magnitude with a two-tailed probability value of 0.02 per cent. The results suggest an anticorrelation between the X-ray and optical data. However, obtaining additional X-ray data from missions such as *AstroSat* will be valuable to obtain a precise cyclic variation of Proxima Centauri.

4 SUMMARY

To summarize,

(i) We have presented the light curves and spectra of Proxima Centauri obtained from the SXT onboard *AstroSat*. The observation was carried out as a part of the simultaneous observational campaign with *Chandra* and *HST*.

(ii) Both SXT and *Chandra* LETG/HRC-S zeroth-order light curves cover a flare-like event.

(iii) The timing behaviour of the flare-like event shows Neupert effect similar to the solar flares where the UV light curve precedes the soft X-ray light curves.

(iv) Three-temperature component models provide the best fit to SXT spectra with sub-solar abundance.

(v) The emission measure distribution model peaks around 1 keV.

(vi) The *AstroSat* quiescent X-ray flux in 0.3–4.0 keV energy range is consistent with previous estimates of quiescent flux.

ACKNOWLEDGEMENTS

This publication uses the data from the AstroSat mission of the Indian Space Research Organisation (ISRO). This work has used the data from the Soft X-ray Telescope (SXT). The SXT POCs at TIFR are thanked for verifying and releasing the data via the ISSDC data archive and providing the necessary software tools. This research has made use of the data and software obtained

from NASA's High Energy Astrophysics Science Archive Research Center (HEASARC), a service of Goddard Space Flight Center and the Smithsonian Astrophysical Observatory. The use of the XRT Data Analysis Software (XRTDAS) developed under the responsibility of the ASI Science Data Center (ASDC) is gratefully acknowledged. This work has made use of observations with *Chandra* and *HST*. This work was also partially supported by a Leverhulme Trust Research Project Grant.

REFERENCES

Agrawal P. C., 2006, Adv. Space Res., 38, 2989
Agrawal P. C., 2017, J. Astrophys. Astron., 38, 27
Alexander T., 1997, in Maoz D., Sternberg A., Leibowitz E. M., eds, Astrophysics and Space Science Library, Vol. 218, Astronomical Time Series. Springer, Berlin, p. 163
Anglada-Escudé G. et al., 2016, Nature, 536, 437
Arnaud K. A., 1996, in Jacoby G. H., Barnes J., eds, ASP Conf. Ser. Vol. 101:, Astronomical Data Analysis Software and Systems V. Astron. Soc. Pac., San Francisco, p. 17
Benz A. O., Güdel M., 2010, ARA&A, 48, 241
Boyajian T. S. et al., 2012, ApJ, 757, 112
Brinkman A. C. et al., 1997, in Hoover R. B., Walker A. B., eds, Proc. SPIE Conf. Ser. Vol. 3113, Grazing Incidence and Multilayer X-Ray Optical Systems. SPIE, Bellingham, p. 181
Brinkman A. C., van Rooijen J. J., Bleeker J. A. M., Dijkstra J. H., Heise J., de Korte P. A. J., Mewe R., Paerels F., 1987, Astrophys. Lett. Commun., 26, 73
Fuhrmeister B., Lalitha S., Poppenhaeger K., Rudolf N., Liefke C., Reiners A., Schmitt J. H. M. M., Ness J.-U., 2011, A&A, 534, A133
Grevesse N., Sauval A. J., 1998, Space Sci. Rev., 85, 161
Güdel M., Audard M., Skinner S. L., Horvath M. I., 2002, ApJ, 580, L73
Güdel M., Audard M., Reale F., Skinner S. L., Linsky J. L., 2004, A&A, 416, 713
Haisch B. M., Linsky J. L., 1980, ApJ, 236, L33
Haisch B. M., Linsky J. L., Bornmann P. L., Stencel R. E., Antiochos S. K., Golub L., Vaiana G. S., 1983, ApJ, 267, 280
Haisch B. M., Butler C. J., Foing B., Rodono M., Giampapa M. S., 1990, A&A, 232, 387
Haisch B., Antunes A., Schmitt J. H. M. M., 1995, Science, 268, 1327
Howard W. S. et al., 2018, ApJ, 860, L30
Kiraga M., Stepien K., 2007, Acta Astron., 57, 149
Lammer H., Selsis F., Ribas I., Guinan E. F., Bauer S. J., Weiss W. W., 2003, ApJ, 598, L121
Lemen J. R., Mewe R., Schrijver C. J., Fludra A., 1989, ApJ, 341, 474
Lim J., White S. M., Slee O. B., 1996, ApJ, 460, 976
MacGregor M. A., Weinberger A. J., Wilner D. J., Kowalski A. F., Cranmer S. R., 2018, ApJ, 855, L2
Neupert W. M., 1968, ApJ, 153, L59
Ottmann R., Schmitt J. H. M. M., 1996, A&A, 307, 813
Reid I. N., Burgasser A. J., Cruz K. L., Kirkpatrick J. D., Gizis J. E., 2001, AJ, 121, 1710
Shapley H., 1951, Proc. Natl. Acad. Sci. USA, 37, 15
Singh K. P., White N. E., Drake S. A., 1996, ApJ, 456, 766
Singh K. P. et al., 2014, Space Telescopes and Instrumentation 2014: Ultraviolet to Gamma Ray, 9144. SPIE, p. 91441S
Singh K. P., et al., 2016, Space Telescopes and Instrumentation 2016: Ultraviolet to Gamma Ray, 9905, SPIE. p. 389
Singh K. P. et al., 2017a, J. Astrophys. Astron., 38, 29
Singh K. P., Dewangan G. C., Chandra S., Bhattacharayya S., Chitnis V., Stewart G. C., Westergaard N. J., 2017b, Curr. Sci., 113, 587
Suárez Mascareño A., Rebolo R., González Hernández J. I., 2016, A&A, 595, A12
van Leeuwen F., 2007, A&A, 474, 653
Voges W. et al., 1996, IAU Circ., 6420, 2
Voges W. et al., 2000, IAU Circ., 7432, 3
Wargelin B. J., Saar S. H., Pojmański G., Drake J. J., Kashyap V. L., 2017, MNRAS, 464, 3281
Wood B. E., Linsky J. L., 2010, ApJ, 717, 1279

This paper has been typeset from a TEX/LATEX file prepared by the author.